An Effective *PQ*-Decoupling Control Scheme Using Adaptive Dynamic Programming Approach to Reducing Oscillations of Virtual Synchronous Generators for Grid Connection with Different Impedance Types

Zhongyang Wang, Youqing Wang*, Senior Member, IEEE, Masoud Davari*, Senior Member, IEEE, and Frede Blaabjerg, Fellow, IEEE

Abstract—The power coupling of the virtual synchronous generator (VSG) in the grid-connected mode may aggravate power oscillation because of a resistance-inductive line. In order to deal with this issue, this research study proposes an adaptive and optimal approach to controlling VSG via reinforcement learning and adaptive dynamic programming (ADP). It derives the linear and nonlinear hybrid equations of the VSG power considering the case where the line impedance is uncertain. The nonlinear part is a disturbance, and the linear ADP solves the optimal feedback control and compensation controller, eliminating the interaction between the active power and reactive power. Also, the proposed method utilizes value iteration and is data-driven. Thus, it does not rely on an initial stability control gain and an accurate dynamic model during the learning process. Comparative experiments reveal the effectiveness of the proposed method and validate the practicability of the methodology introduced; additionally, comparative simulations present the superiority of the proposed method in power systems based on synchronous generators.

Index Terms—Adaptive dynamic programming (ADP), coupling between active power and reactive power, linear-quadratic regulator (LQR), optimal feedback controller, value iteration, virtual synchronous generator (VSG).

The work of Youqing Wang was supported by the National Science Fund for Distinguished Young Scholars under Grant 62225303; the Fundamental Research Funds for the Central Universities (buctrc202201); China Scholarship Council; and High Performance Computing Platform, College of Information Science and Technology, Beijing University of Chemical Technology. The work of Masoud Davari was supported in part by the U.S.-Denmark program between Georgia Southern University, Statesboro, GA, USA, and Aalborg University, Aalborg, Denmark, funded by the International Research Experiences for Students (IRES) program in Office of International Science and Engineering in the U.S. National Science Foundation (U.S. NSF) under U.S. NSF OISE-IRES Award #2152905, in part by the U.S. NSF under ECCS-EPCN Awards #1808279 and #1902787, and in part by the dSPACE company, Verivolt company, the professional development part of Masoud Davari's Discovery & Innovation Award from the 2020-2021 University Awards of Excellence at Georgia Southern University, and his 2022 Impact Area Accelerator Grant partially funded by Georgia Southern Universityat which all experiments were conducted. (*Corresponding authors: Youqing Wang; Masoud Davari.)

Zhongyang Wang and Youqing Wang are with the College of Information Science and Technology, Beijing University of Chemical Technology, Beijing 100029, China (e-mail: wangzhongyang@buct.edu.cn; wang.youqing@ieee.org).

Masoud Davari is with the Department of Electrical and Computer Engineering, Georgia Southern University University (Statesboro), Statesboro, GA 30460 USA (e-mail: mdavari@georgiasouthenr.edu; davari@ualberta.ca).

Frede Blaabjerg is with the AAU Energy Department, Aalborg University, Aalborg 9220, Denmark (e-mail: fbl@energy.aau.dk).

I. Introduction

THE penetration rate of distributed renewable energy generation in power systems has recently increased annually. The grid-connected inverter converts dc energy to ac energy from a source; it is also the core equipment for connecting distributed power to power networks [1]–[3]. However, due to the intermittency and randomness of the power system and the grid connection of new energy generation, several grid-connected power-electronic devices have almost no inertia and damping characteristics. Consequently, they bring significant challenges to the operation of the grid. Therefore, some experts and scholars have put forward the virtual synchronous generators (VSGs); see [4] and references therein.

A VSG also provides active and reactive droop control modules to support the power grid. Concurrently, by introducing mechanical equations, the transient response characteristics of the grid-connected converter are improved, thereby enhancing the system's inertia [5]–[7]. A VSG allows the grid-connected inverter to have the steady-state characteristics of droop control and simulates the dynamic frequency response characteristics of a synchronous generator. Also, the droop control embedded in VSG improves the antidisturbance capability of the system and addresses underdamped and low-inertia problems [8].

The rotor oscillation characteristic of a synchronous generator is inevitably brought about by introducing inertia. In order to suppress the VSG transient active power oscillation without increasing the steady-state deviation, research has been conducted into three major categories—as detailed in this and the following two paragraphs. The first type is based on the adaptive inertia damping method [9]–[12].

In [9], the expected inertia in the power-oscillation process has been determined from the VSG power-angle curve; a bangbang-control-based strategy using alternating inertia has been proposed in order to improve the system's transient characteristics. Nevertheless, this control method introduces unnecessary nonlinearity, which affects the system's performance. In [11] and the arXiv review work [10], the authors have considered the influence of damping and proposed a control strategy in which inertia and damping have been adaptively altered. In [12], the authors determined different damping and inertia according to various frequency errors and changes. This

control method must detect all frequency changes, and the control process is more complicated. Additionally, improper selection of the frequency offset threshold leads to the so-called "jitter" problem of the virtual inertia value in the dynamic process, thus affecting the system's stability.

The second type of control method introduces a control link to improve the transient characteristics and ensure that the inertia damping remains unchanged—unlike the adaptive inertia damping method. In [13], the transient equivalent damping has been improved by introducing a differential link to achieve oscillation suppression. Still, the differential method will cause a huge high-frequency interference problem, which is generally not used in engineering practice. In [14], the authors have constructed a transient damping method employing the band-pass damping algorithm; it leads to a higher-order system—thereby quickly causing power shock, triggering overcurrent protection, and endangering the reliable operation of the system. Active disturbance rejection control (ADRC) technology is applied to the VSG in [15]. However, the ADRC is not applied to the power loop and cannot improve the transient performance of the system. Model predictive control (MPC) is utilized to design the controller to improve the VSG frequency and voltage performance [16]. Still, the MPC method requires several calculations and high real-time performance of the system.

The third type of control method is to add a secondary frequency controller. The secondary control frequency and voltage recovery have been studied in [17], [18]. Still, in microgrid modeling, the dynamic characteristics of the LC filter, local load, and distribution network are often ignored. In [19], the active power-frequency response model is incorporated in the secondary frequency control. In this method, distributed generation and energy storage units are equivalent to an inertial link with a time constant. Nevertheless, this method is unsuitable because of the coupling between frequency and power in a low-voltage microgrid.

Literature shows that conventional VSGs suffer from power coupling, which needs to be tackled as effectively as possible. Large inductance is usually introduced to reduce coupling. This effort increases the line voltage drop and total cost. However, in low-voltage microgrids, the line impedance is resistive; there is a significant coupling phenomenon associated with the VSG power, which reduces the system's stability and control performance, thereby affecting the power quality [20], [21]. In order to make the line inductive, an inductor can be placed in series with the line. Nevertheless, this increases the process complexity and the design cost. In [22], [23], the authors added a virtual impedance to the control loop to maximize the line inductance ratio. Although this method can effectively eliminate the influence of an extensive line impedance ratio on the power coupling, the approximate decoupling method can only be achieved by relying on the assumption that "the power angle is approximately zero."

In [24], the decoupling current has been introduced in the current loop to resolve the decoupling issue. Still, a significant power disturbance will cause large current fluctuations and impact the system's stability. In [25], the traditional droop control is introduced into coordinate transformation to adapt

to the coupling effect caused by a large impedance ratio. Nonetheless, this method is very susceptible to the line impedance ratio. Some researchers have proposed a power decoupling method based on a compensation matrix; see [26]. In this approach, the reference voltage value is corrected by a particular inverse matrix to counteract the inductive coupling of the control equipment. However, this method is complex and needs to be more intuitive. In [27], the authors have considered the power angle and proposed a more accurate power decoupling control strategy. In this methodology, the VSG's small signal model has been established near the stable operating point to design the power decoupling strategy. However, when the operating point is disturbed in an extensive range, the control effect will be reduced. Another drawback of the above research is that it requires an accurate mathematical model of the system to design the control. In this regard, it is noteworthy that developing approaches to designing controllers for the systems whose models are unknown or not needed is practically more attractive and suitable.

The authors of [28] have introduced a synchronous virtual impedance to reduce the high line impedance ratio R/X. Then the VSG small signal model is established to realize power decoupling; this method requires the assumption that the power angle is approximately zero, so there are solutions better than the one proposed in [28]. As a result, it is not the optimal solution. The authors of [29] have proposed using current decoupling instead of power decoupling, thus requiring to measure the current directly to decouple active and reactive power. If this method is utilized, the system design will become more complex.

In order to solve the power coupling problem under the unknown system model, this study proposes a novel reinforcement learning (RL) approach—see [30]—it also introduces the adaptive dynamic programming (ADP) method to improve VSG performance. The reason behind deploying the RL theory is as follows. It describes and solves the problem based on agents employing learning strategies to accomplish specific goals or maximize returns while interacting with the environment. In actual application, RL has made relevant achievements, such as power and electronic system [31], vehicles [32], and robotic manipulation [33]. The ADP algorithm synthesizes and generates an adaptive and optimal control for dynamic systems with unknown parameters [34]-[37]. In [37], [38], the author uses the policy iteration (PI) method to implement ADP; the PI method is easy to implement, and policy and value can be updated at the same time. However, the PI method requires an initial stability control gain; even if the system is known, the initial stability control gain is not easy to obtain. In contrast, the value iteration (VI) method does not rely on the initial stability gain in the implementation of ADP [39]. Therefore, this study uses the VI method.

In [40], the authors applied the ADP approach to controlling the VSG active power for the first time; this method has achieved several good results. In [41], the authors studied the optimal frequency control for the VSG via the ADP. Still, it is based on the zero power angle—which is an approximation—an inductive line impedance, and the simple linear equation of the VSG. Herein, however, the VSG dynamics are represented

by a combination of linear and nonlinear states. The linear part obtains the optimal feedback gain through the ADP, and the nonlinear part acts as a disturbance. Additionally, a compensation controller eliminates the coupling between the active power and reactive power (hereinafter referred to "active and reactive power" for simplicity). In order to make a comparison when the line is mainly resistive, different methods of conventional VSGs, virtual impedance increase, and the method proposed in [40] (under the virtual impedance increase condition) are designed and simulated.

Compared with the state-of-the-art research on the theme targeted in this paper [10], [26]–[29], [40], [42], [43], this paper's main novelties are as follows.

- In [10], the authors have introduced an adaptive virtual inertial control for VSG, which may cause parameter jitter-related problems near the critical value. The proposed method's control parameters are not required to be changed frequently. As a result, it has less sophistication and no jitter-related problems.
- 2) In [26], [27], the authors have proposed a power decoupling method to reduce the coupling between active and reactive power. Therein, their approach has been based on replacing the original nonlinear model with an approximate linear model, thus reducing the model's accuracy under a wide range of changes in the operating point. However, the technique introduced herein considers the original VSG's mathematical model and achieves reasonably good results under a wide range of changes in the operating point.
- 3) In [28], [40], the researchers have assumed an approximate decoupling between active and reactive power—considering that the power angle is zero—so this consideration makes the problem under study specific. However, in practical power networks, the power angle cannot either be ignored or be approximated by zero. The method proposed in this research eliminates the above assumption that the power angle is zero. As a result, the proposed solution is optimal for many cases—not a particular case.
- 4) Compared with the review work of [29], the proposed VSG control system does not require the direct measurement of the current to decouple active and reactive power, thus reducing the measurement sensors and their associated costs.
- Compared with [42], this paper presents a new reactivepower-voltage loop that is entirely identical to the activepower-frequency loop—thus simplifying the selection of parameters.
- 6) In [43], the authors have proposed a VSG control algorithm based on the linear-quadratic regulator (LQR). This method requires approximate linearization and accurate known parameters. The methodology proposed in this paper is based on a data-driven and optimal control, so it does not require a precise mathematical model of the system to synthesize the optimal VSG controller.

Consequently, according to the state-of-the-art scholarly work reviewed in this paper, the contributions of this study can be summarized as follows.

- Firstly, this paper designs a VSG decoupling control method based on ADP control for the first time. Physical analysis of the nature of power coupling has promoted the understanding and development of VSG technology.
- Secondly, the method proposed in this article relaxes the zero power angle restriction discussed above, so it applies to more general situations.
- Thirdly, this paper designs a new reactive voltage loop control loop, which is symmetric to the active frequency loop, thereby simplifying the parameter design.
- 4) Ultimately, the method proposed in this article is datadriven and does not rely on exact mathematical models.

The rest of this paper is organized as follows. Section II introduces the problems of conventionally controlled VSGs. Section III introduces the VSG improvement process in detail and deduces the design for the compensation controller. Section IV details the LQR problem and the ADP approach using the VI algorithm to find the optimal feedback gains for the unknown dynamic model of a VSG recursively. Section V presents the experiments conducted in order to display comparative results (compared with other traditional VSG control methods) and reveal the practicality and feasible implementation of the proposed method. Section VI concludes this paper's outcomes, findings, and contributions to the field under investigation.

Notations. In this paper, the following notations are defined.

$$\operatorname{vecs}(P) = [p_{11}, 2p_{12}, \cdots, 2p_{m-1,m}, p_{mm}]^T \in \mathbb{R}^{\frac{1}{2}m(m+1)},$$

$$\operatorname{vec}(Y) = [y_1^T, y_2^T, \cdots, y_m^T]^T \in \mathbb{R}^{mn},$$

$$\operatorname{vecv}(v) = [v_1^2, v_1 v_2, \cdots, v_1 v_n, v_2^2, v_2 v_3, \cdots, v_{n-1} v_n, v_n^2]^T \in \mathbb{R}^{\frac{1}{2}n(n+1)},$$

$$\operatorname{vec}(ABC) = (C^T \otimes A)\operatorname{vec}(B) \in \mathbb{R}^{nr}$$

where \otimes indicates the Kronecker product operator. $P \in \mathbb{R}^{m \times m}$, $Y \in \mathbb{R}^{n \times m}$, $v \in \mathbb{R}^n$, $A \in \mathbb{R}^{n \times m}$, $B \in \mathbb{R}^{m \times q}$, and $C \in \mathbb{R}^{q \times r}$.

II. PROBLEMS WITH CONVENTIONAL VSG

A. Algorithm of Conventional VSG

Figure 1 displays the topology and control block diagram of a conventional VSG. $V_{\rm dc}$ is the dc-side voltage; I_g is the grid current respectively; V_s and V_g are the converter output voltage (also the VSG output voltage) and the grid voltage respectively; L_f , R_f and L_g , R_g are the inverter side and line impedances, respectively; C is the filter capacitor.

The VSG algorithm module includes an active power loop (APL) and reactive power loop (RPL). This module comes up with the amplitude and phase angle of the inverter output voltage through active-frequency and reactive-voltage control. The VSG control is expressed by

$$\begin{cases} \dot{\delta} = \omega - \omega_g \\ J_p \dot{\omega} = P_{\text{ref}} - P_{\text{e}} - D_p (\omega - \omega_o) \\ V_s = V_g + \left(K_p + \frac{K_i}{s} \right) (Q_{\text{ref}} - Q_{\text{e}}) \end{cases}$$
(1)

where P_{ref} and Q_{ref} are the input reference power; P_{e} and Q_{e} denote the output power; δ is the power angle; ω and

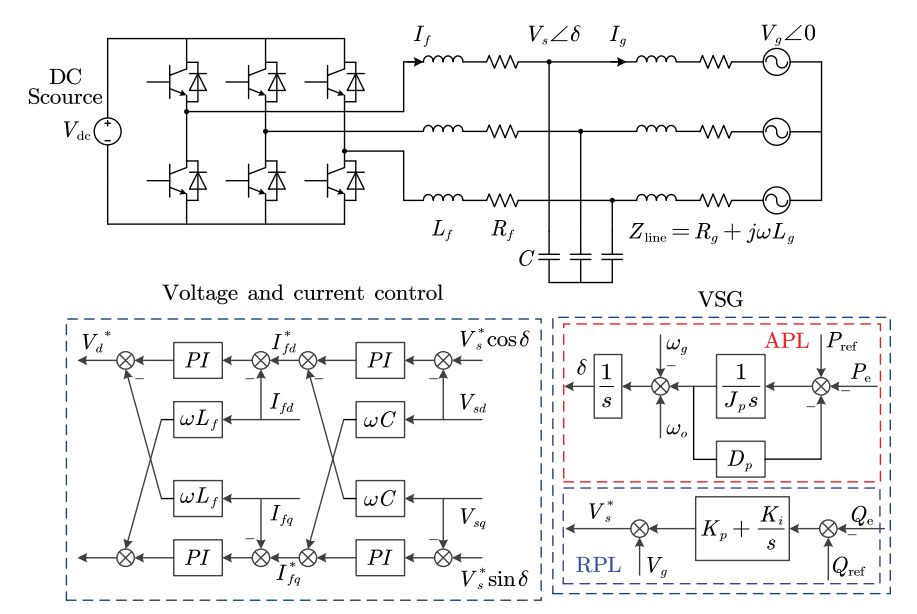


Fig. 1. Topology and control block diagram of conventional VSG.

 ω_n are the output angular frequency and reference angular frequency (grid angular frequency), respectively; J_p and D_p are the virtual inertia and droop coefficients of APL, respectively; K_p and K_i are the reactive power adjustment factor of RPL, respectively.

B. Oscillation Analysis of Conventional VSG

The power calculation method is expressed by

$$\begin{cases} P_{\rm e} = 1.5 V_g V_s \cos(\alpha - \delta) / Z_{\rm line} - 1.5 V_g^2 \cos\alpha / Z_{\rm line} \\ Q_{\rm e} = 1.5 V_g V_s \sin(\alpha - \delta) / Z_{\rm line} - 1.5 V_g^2 \sin\alpha / Z_{\rm line} \end{cases}$$
(2)

where $Z_{\text{line}} = \sqrt{R_g^2 + (\omega_g L_g)^2}$ (shown in Fig. 1), and $\alpha = \arctan(\omega_g L_g/R_g)$; see [23]. Hereinafter, $Z_{\text{line}} \triangleq Z$ for ease of reference in the upcoming equations.

The equivalent impedance of power transmission and distribution lines exhibits different characteristics; the resistance angle α of the line varies between 0° and 90° . The power angle is relatively small, it can approximately be considered $\sin\delta\approx\delta$ and $\cos\delta\approx1$. The VSG active and reactive power are expressed by

$$P_{\rm e} = 1.5 V_{\rm g} V_{\rm s} \delta / Z$$
, and $Q_{\rm e} = 1.5 V_{\rm g} (V_{\rm s} - V_{\rm g}) / Z$. (3)

Equation (3) reveals the VSG active and reactive power are decoupled, enabling their control by changing the frequency and amplitude, respectively.

When the resistive component of the line impedance cannot be ignored, (2) shows that the VSG active and reactive power are related to the power angle and voltage amplitude, and a strong coupling relationship exists. When the system fluctuates, the system small-signal model is expressed by

$$\Delta P_{\rm e} = m_{n\delta} \Delta \delta + m_{pV_s} \Delta V_s$$
 and $\Delta Q_{\rm e} = m_{a\delta} \Delta \delta + m_{aV_s} \Delta V_s$ (4)

where $m_{p\delta}=1.5V_gV_{so}\sin(\alpha-\delta_o)/Z$, $m_{pV_s}=1.5V_g\cos(\alpha-\delta_o)/Z$, $m_{q\delta}=-1.5V_gV_{so}\cos(\alpha-\delta_o)/Z$, and $m_{qV_s}=1.5V_g\sin(\alpha-\delta_o)/Z$. $\Delta P_{\rm e}$ and $\Delta Q_{\rm e}$ are the variations of the VSG active and reactive power, respectively.

 V_{so} and δ_o are the steady-state operating point of the output voltage and power angle, respectively. Equation (4) reveals that the change in one power will cause the change in the other. As a result, the mutual coupling will increase the risk of oscillations and overcurrent in the system.

C. Influence of Grid Frequency Fluctuation in Power

A change in the frequency will cause a variation in the power angle, leading to an oscillation of active and reactive power. Assuming that the grid frequency deviation is $\Delta \omega_g = \omega_g - \omega_o$, from (1) and (4), transfer functions of active power/frequency and reactive power/frequency are found as

$$\begin{cases} \frac{\Delta P_{\rm e}}{\Delta \omega_g} = -\frac{D_p m_{p\delta}}{J_p s^2 + D_p s + m_{p\delta}} + \frac{J_p m_{p\delta} s^2 + D_p m_{p\delta} s}{J_p s^2 + D_p s + m_{p\delta}} \frac{\Delta V_s}{\Delta \omega_g} \\ \frac{\Delta Q_{\rm e}}{\Delta \omega_g} = \frac{m_{q\delta} (\Delta \omega - \Delta \omega_g)}{\Delta \omega_g [(m_{qV_s} k_p + 1) s + m_{qV_s} k_i]} \end{cases}$$
(5)

Consequently, the following conclusion can be drawn.

$$\lim_{t \to \infty} \Delta P_{\rm e} = -D_p \Delta \omega_g \text{ and } \lim_{t \to \infty} \Delta Q_{\rm e} = 0. \tag{6}$$

III. IMPROVED VSG CONTROL

A. Differential Equations of VSG

The conventional VSG ignores the line impedance influence and approximates active and reactive power coupling. Thus, an inevitable coupling between active and reactive power exists in the actual process. As a result, when the power changes, the conventional VSG produces larger oscillations.

This paper first redefines the VSG control scheme as

$$\dot{\delta} = \Delta\omega - \Delta\omega_g, \Delta\dot{\omega} = u_1, \frac{\dot{V}_s}{V_s} = \Delta d, \Delta\dot{d} = u_2. \tag{7}$$

The time derivatives of $P_{\rm e}$ and $Q_{\rm e}$ from (2) are as

$$\begin{split} \dot{P}_{\mathrm{e}} &= (Q_{\mathrm{e}} + a) \left(\Delta \omega - \Delta \omega_{\mathrm{g}} \right) + (P_{\mathrm{e}} + b) \Delta d, \text{ and} \\ \dot{Q}_{\mathrm{e}} &= - \left(P_{\mathrm{e}} + b \right) \left(\Delta \omega - \Delta \omega_{\mathrm{g}} \right) + \left(Q_{\mathrm{e}} + a \right) \Delta d \end{split} \tag{8}$$

where $a = 1.5V_g^2 \sin \alpha/Z$ and $b = 1.5V_g^2 \cos \alpha/Z$.

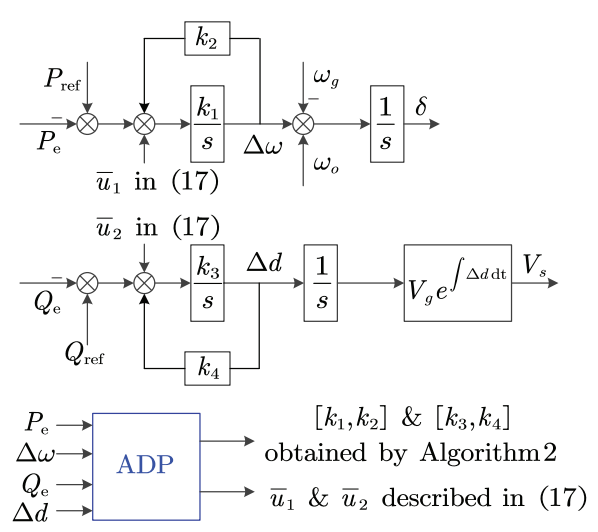


Fig. 2. Detailed diagram of the proposed method.

Now, assuming $x = \begin{bmatrix} P_e & \Delta\omega & Q_e & \Delta d \end{bmatrix}^T$, the VSG's nonlinear dynamics in the state-space representation are expressed by (9) and (10).

$$\begin{cases} \dot{x}_1 = ax_2 + bx_4 + f_1 \\ \dot{x}_2 = u_1 \\ \dot{x}_3 = -bx_2 + ax_4 + f_2 \\ \dot{x}_4 = u_2 \end{cases}$$
 (9)

where $f_1 \triangleq x_1x_4 + x_3x_2$ and $f_2 \triangleq x_3x_4 - x_1x_2$ are nonlinear terms.

Obviously, the APL and RPL loops are entirely identical. Now, the APL dynamics are

$$\dot{x}_{p} = A_{p}x_{p} + B_{p}u_{1} + D_{p}v_{p} + H_{p}f_{1}$$
where $x_{p} = \begin{bmatrix} x_{1} \\ x_{2} \end{bmatrix}$, $v_{p} = \begin{bmatrix} x_{4} \\ 0 \end{bmatrix}$, $A_{p} = \begin{bmatrix} 0 & a \\ 0 & 0 \end{bmatrix}$,
$$B_{p} = \begin{bmatrix} 0 \\ 1 \end{bmatrix}$$
, $D_{p} = \begin{bmatrix} b \\ 0 \end{bmatrix}$, and $H_{p} = \begin{bmatrix} 1 \\ 0 \end{bmatrix}$.

B. Proposed Controller Design for VSG

For the APL and RPL parts, the controller is described as

$$\begin{cases} u_1 = -k_1(P_e - P_{ref}) - k_2 \Delta \omega + \bar{u}_1 = \hat{u}_1 + \bar{u}_1 \\ u_2 = -k_3(Q_e - Q_{ref}) - k_4 \Delta d + \bar{u}_2 = \hat{u}_2 + \bar{u}_2 \end{cases}$$
(11)

Then, the second-order transfer functions for the active and reactive power are obtained and expressed in (12) and (13).

$$s^{2}P_{e} = -ak_{1}(P_{e} - P_{ref}) - k_{2}(sP_{e} - b\Delta d - f_{1}) + a\bar{u}_{1}$$

$$+ b(\hat{u}_{2} + \bar{u}_{2}) + sf_{1}.$$
(12)

and

$$s^{2}Q_{e} = -ak_{3}(Q_{e} - Q_{ref}) + a\bar{u}_{2} - b(\hat{u}_{1} + \bar{u}_{1}) + sf_{2} -k_{4}(sQ_{e} + b(\Delta\omega - \Delta\omega_{g}) - f_{2}).$$
(13)

Then, one has

$$P_{e} = \frac{ak_{1}}{s^{2} + k_{2}s + ak_{1}} P_{ref} + \underbrace{\frac{\bar{u}_{1}}{s^{2} + k_{2}s + ak_{1}}}_{(14)} + \underbrace{\frac{\bar{u}_{1}}{s^{2} + k_{2}s + ak_{1}}}_{(14)},$$

and

$$Q_{e} = \frac{ak_{3}}{s^{2} + k_{4}s + ak_{3}} Q_{ref} + \frac{a\bar{u}_{2} - b\bar{u}_{1}}{s^{2} + k_{4}s + ak_{3}} + \frac{\tilde{u}_{2}}{-b\hat{u}_{1} + k_{4}(-b(\Delta\omega - \Delta\omega_{g}) + f_{2}) + sf_{2}}}{s^{2} + k_{4}s + ak_{3}}.$$
(15)

In order to eliminate the coupling between the active and reactive power, the following relationship must be satisfied.

$$a\bar{u}_1 + b\bar{u}_2 + \tilde{u}_1 = 0$$
, and $a\bar{u}_2 - b\bar{u}_1 + \tilde{u}_2 = 0$. (16)

Consequently, the compensation controllers for the APL and RPL are

$$\bar{u}_1 = \frac{-a\tilde{u}_1 + b\tilde{u}_2}{a^2 + b^2}$$
, and $\bar{u}_2 = \frac{-b\tilde{u}_1 - a\tilde{u}_2}{a^2 + b^2}$. (17)

The improved VSG control is expressed by

$$\begin{cases} \delta = \int (\omega - \omega_g) dt \\ \dot{\omega} = k_1 (P_{\text{ref}} - P_e) - k_2 (\omega - \omega_o) + \bar{u}_1 \end{cases}, \tag{18}$$

and

$$\begin{cases} V_s = V_g e^{\int \Delta d dt} \\ \Delta \dot{d} = k_3 (Q_{\text{ref}} - Q_e) - k_4 \Delta d + \bar{u}_2 \end{cases}$$
 (19)

Equation (19) reveals the new realization method for the reactive-power-voltage loop as one of the contributions of this paper pointed out in the introduction section. Finally, Fig. 2 depicts the control block diagram of the method proposed in this paper. The control parameters k_1 , k_2 , k_3 , and k_4 can be obtained in Section IV.

IV. ADP-BASED VSG CONTROL ALGORITHM

A. Problem Description and LQR

Consider the VSG hybrid equation described as

$$\begin{cases} \dot{x} = Ax + Bu + Dv + Hf \\ u = -K\Delta x + \bar{u} \end{cases}$$
 (20)

where $x \in \mathbb{R}^n$, $u \in \mathbb{R}^m$, $v \in \mathbb{R}^w$, $f \in \mathbb{R}^q$, $A \in \mathbb{R}^{n \times n}$, $B \in \mathbb{R}^{n \times m}$, $D \in \mathbb{R}^{n \times q}$, and $K \in \mathbb{R}^{m \times n}$.

The control objective is that Problem 1 synthesizes the optimal feedback gain K.

Problem 1.

$$\min_{u} \int_{t}^{+\infty} (\Delta x(\tau)^{T} (Q + K^{T} R K) \Delta x(\tau)) d\tau$$
subject to (20)

where $Q = Q^T \ge 0$, $R = R^T \ge 0$, and (A, \sqrt{Q}) is observable.

Equation (22) finds the feedback gain, as Problem 1 is an LQR problem.

$$K = R^{-1}B^TP \tag{22}$$

where $P = P^T > 0$ is a positive definite matrix and the unique solution to the following Lyapunov equation.

$$A^{T}P + PA + Q - PBR^{-1}B^{T}P = 0. (23)$$

Algorithm 1 Value Iteration Algorithm

Initialization: Choose $P_0 = P_0^T > 0$, $j, q \leftarrow 0$, and $\tau > 0$. **Value Evaluation**: Solve for \bar{P}_{j+1} using

$$\bar{P}_{i+1} = P_i + \varepsilon_i (A^T P_i + P_i A + Q - P_i B R^{-1} B^T P_i). \tag{25}$$

If $\bar{P}_{j+1} \notin B_q$, then, $P_{j+1} \leftarrow P_0$, $q \leftarrow q+1$, else if $|\bar{P}_{j+1} - P_j|/\varepsilon_j < \tau$ then return $P_j = P^*$ and go to Policy Improvement. else $P_{j+1} \leftarrow \bar{P}_{j+1}$, end if $k \leftarrow k+1$ and go to Value Evaluation.

Policy Improvement: Update the feedback gain matrix by

$$K^* = R^{-1}B^T P^*. (26)$$

The ball of B_q and the step size of ε_j (see [39]) are defined as

$$B_{q} \subseteq B_{q+1}, \quad q \in \mathbb{N}, \quad \lim_{q \to \infty} B_{q} = \mathbb{P}_{+}^{n}$$

$$\varepsilon_{j} > 0, \quad \sum_{j=0}^{+\infty} \varepsilon_{j} = +\infty, \text{ and } \sum_{j=0}^{+\infty} \varepsilon_{j}^{2} < +\infty.$$
(24)

B. ADP Approach Using the VI Algorithm

First, define $u = u_0$, in which u_0 can be chosen as any initializing control policy. Next, the system in (20) can be rewritten as

$$\dot{x} = Ax + Bu_0 + Dv + Hf. \tag{27}$$

Next, taking the time derivative of $x^T P_i x$ results in

$$\frac{d}{dt}x^{T}P_{j}x = x^{T}Q_{j}x + 2u_{0}^{T}RK_{j}x + 2v^{T}D^{T}P_{j}x + 2f^{T}H^{T}P_{j}x$$
 (28)

where $Q_j = A^T P_j + P_j A$, and $RK_j = B^T P_j$.

During the period of $[t, t + \delta t]$, (28) is rewritten as

$$x^{T}P_{j}x\Big|_{t}^{t+\delta t} = \int_{t}^{t+\delta t} x^{T}Q_{j}xd\tau + 2\int_{t}^{t+\delta t} u_{0}^{T}RK_{j}xd\tau + 2\int_{t}^{t+\delta t} v^{T}D^{T}P_{j}xd\tau + 2\int_{t}^{t+\delta t} f^{T}H^{T}P_{j}xd\tau.$$
(29)

Considering $t_0 \le t_1 \le t_2 \cdots \le t_s$, the following matrices are defined.

$$I_{x,x} = \begin{bmatrix} \int_{t_0}^{t_1} \operatorname{vecv}(x) d\tau, \cdots, \int_{t_{s-1}}^{t_s} \operatorname{vecv}(x) d\tau \end{bmatrix}^T,$$

$$I_{x,u_0} = \begin{bmatrix} \int_{t_0}^{t_1} x \otimes Ru_0 d\tau, \cdots, \int_{t_{s-1}}^{t_s} x \otimes Ru_0 d\tau \end{bmatrix}^T,$$

$$I_{x,v} = \begin{bmatrix} \int_{t_0}^{t_1} x \otimes v d\tau, \cdots, \int_{t_{s-1}}^{t_s} x \otimes v d\tau \end{bmatrix}^T,$$

$$I_{x,f} = \begin{bmatrix} \int_{t_0}^{t_1} x \otimes f d\tau, \cdots, \int_{t_{s-1}}^{t_s} x \otimes f d\tau \end{bmatrix}^T, \text{ and }$$

$$\Gamma_{x,x} = \begin{bmatrix} \operatorname{vecv}(x) |_{t_0}^{t_1}, \cdots, \operatorname{vecv}(x) |_{t_{s-1}}^{t_{s-1}} \end{bmatrix}^T.$$

Then, (29) represents a linear matrix equation form expressed by

$$\Psi_i \Phi_i = \Gamma_{x,x} \text{vecs}(P_i) \tag{30}$$

Algorithm 2 Adaptive and Optimal Controller Design

Initialization: Choose $P_0 = P_0^T > 0$, initial control strategy $u_0(t)$ $j, q \leftarrow 0$, and $\tau > 0$

Data Collection: Collect online data: $I_{x,x}$, I_{x,u_0} , $I_{x,f}$, $I_{x,v}$ and $\Gamma_{x,x}$.

Solve for Q_j and K_j using (32). Then solve for \bar{P}_{j+1} using:

$$\bar{P}_{j+1} = P_j + \varepsilon_j (Q_j + Q - K_j^T R K_j). \tag{33}$$

If $\bar{P}_{j+1} \notin B_q$, then $P_{j+1} \leftarrow P_0$, $q \leftarrow q+1$, else if $|\bar{P}_{j+1} - P_j|/\varepsilon_j < \tau$, then $P_j = P_{j^*}$ and $K_j = K_{j^*}$.

where $\Phi_j = [\text{vecs}(Q_j)^T, \text{vec}(K_j)^T, \text{vec}(D^T P_j)^T, \text{vec}(H^T P_j)^T]^T$, and $\Psi_j = \begin{bmatrix} I_{x,x} & 2I_{x,u_0} & 2I_{x,y} & 2I_{x,f} \end{bmatrix}$.

Matrix Ψ_j is required to be a full rank matrix to ensure that the linear equation (30) has a unique solution, as detailed in (31).

$$\operatorname{rank}(\Psi_j) = \frac{n(n+1)}{2} + mn + wn + qn. \tag{31}$$

The unique solution to (30) under (31) is

$$\Phi_j = (\Psi_j^T \Psi_j)^{-1} \Psi_j \Gamma_{x,x} \text{vecs}(P_j). \tag{32}$$

Lemma 1. While ensuring the algorithm convergence, the solution to (23) can be approximated considering $\{P_j\}$ and $\{K_j\}$ detailed in Algorithm 1 and Algorithm 2. Consequently, $\lim_{j\to\infty}P_j=P_{j^*}$ and $\lim_{j\to\infty}K_j=K_{j^*}$ are concluded [39].

Assuming
$$P_j = \begin{bmatrix} p_{11j} & p_{12j} \\ p_{12j} & p_{22j} \end{bmatrix}$$
, $Q_j = \begin{bmatrix} q_{11j} & q_{12j} \\ q_{12j} & q_{22j} \end{bmatrix}$, and $(D^T P_j)^T = \begin{bmatrix} d_{1j} \\ d_{2j} \end{bmatrix}$, the following is derived and concluded.

$$A^{T}P_{j} + P_{j}A = \begin{bmatrix} 0 & ap_{11j} \\ ap_{11j} & 2ap_{12j} \end{bmatrix} = Q_{j}, \text{ and}$$

$$(D^{T}P_{j})^{T} = \begin{bmatrix} bp_{11j} \\ bp_{12j} \end{bmatrix} = \begin{bmatrix} d_{1j} \\ d_{2j} \end{bmatrix}.$$
(34)

By (34), the system parameters a and b are described as

$$a = \frac{q_{12j}}{p_{11j}}$$
, and $b = \frac{d_{1j}}{p_{11j}}$. (35)

C. Rigorous Stability Analysis of Proposed VSG Control

This subsection elaborates on the rigorous stability and convergence of the proposed VSG control via the following subsubsection detailing Theorems 2 and 1.

1) ADP Convergence of the Proposed ADP-Based VSG Control:

Theorem 1. The equations $\lim_{j\to\infty} P_j = P_{j^*}$ and $\lim_{j\to\infty} K_j = K_{j^*}$ are valid, provided that (31) is satisfied. As a result, the convergence of $\{P_j\}$ and $\{K_j\}$ is guaranteed according to Algorithm 2.

Proof. The unique solution (Q_j, K_j) for (32) will exist, provided that (31) is satisfied. **Value Evaluation** in Algorithm 2 is able to determine P_{j+1} and \bar{P}_{j+1} uniquely; they are equivalent to the ones in Algorithm 1. **Lemma 1** proves the convergences of $\{P_j\}$ and $\{K_j\}$. The **Theorem 1** proof is now completed.

2) Stability of the Proposed ADP-Based VSG Control:

Theorem 2. Through the ADP algorithm proposed in this paper, the controller $u = -K_j^* x + \bar{u}$ is able to make the error convergence to 0—i.e., $\lim_{t\to\infty} \Delta P = 0$.

Proof. The closed-loop dynamics of system (20) under $u = -K_i^* x + \bar{u}$ is expressed as

$$\Delta \dot{x} = (A - BK_i^*)\Delta x \tag{36}$$

where $\Delta x = [\Delta P, \Delta \omega]$. Now, a Lyapunov function can be defined as

$$V(x) = \Delta x^T P_i^* \Delta x,\tag{37}$$

where P_j^* is the solution to the Lyapunov equation (23). Thus, the time derivative of V(x) is

$$\dot{V}(x) = \Delta \dot{x}^T P_j^* \Delta x + \Delta x^T P_j^* \Delta \dot{x}
= \Delta x^T ((A - BK_j^*)^T P_j^* + P_j^* (A - BK_j^*)) \Delta x
= -\Delta x^T (Q + K_j^{*T} RK_j^*) \Delta x.$$
(38)

Since Q and R are both positive definite symmetric matrices, one obtains (39).

$$\dot{V}(x) \le 0. \tag{39}$$

Based on (39), $\Delta x = 0$ if and only if the equal sign in (39) is true. According to the Lyapunov stability theorem, the equilibrium state Δx is uniformly asymptotically stable. As a result, one will conclude that $\lim_{t\to\infty} \Delta x = 0$ and $\lim_{t\to\infty} P_e = P_{\text{ref}}$. \square

3) Performance of the Proposed ADP-Based VSG Control: Through the ADP algorithm, $A - BK_j$ is a Hurwitz (or Routh-Hurwitz) matrix. Assuming $K_j = \begin{bmatrix} k_1 & k_2 \end{bmatrix}$, one reaches (40)

$$|s \times I_2 - (A - BK_j)| = s^2 + 2\xi \omega_n s + \omega_n^2$$
 (40)

where I_2 is the identity matrix of size 2 (i.e., the 2×2 square matrix with ones on the main diagonal and zeros elsewhere) $\omega_n=\sqrt{ak_1}$ and $\xi=k_2/2\sqrt{ak_1}$. The two characteristic roots of (40) are

$$s_{1,2} = -\frac{k_2}{2} \pm \frac{\sqrt{|k_2^2 - 4ak_1|}}{2}i. \tag{41}$$

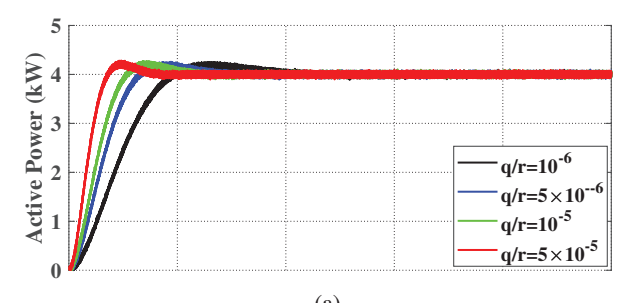
Now, assuming $Q = \begin{bmatrix} q & 0 \\ 0 & q \end{bmatrix}$ and R = r, one obtains (42) using (23).

$$k_1 = \sqrt{\frac{q}{r}}$$
 and $k_2 = \sqrt{2a\sqrt{\frac{q}{r}}}$. (42)

As a result, (41) can be rewritten as

$$s_{1,2} = -\frac{1}{2}\sqrt{2a\sqrt{\frac{q}{r}}} \pm \frac{1}{2}\sqrt{2a\sqrt{\frac{q}{r}}}2i.$$
 (43)

If appropriate weight matrices of Q and R are selected, the VSG system will achieve a satisfactory performance with rigorous stable. Additionally, the ADP algorithm obtains the



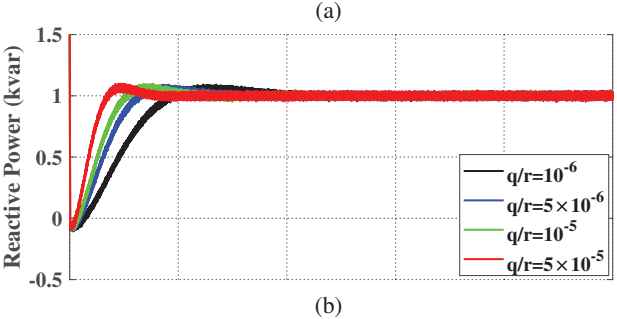


Fig. 3. Time response of the proposed ADP-based VSG control under different control parameters: (a) Active power with the vertical axis of 1 kW/div and the horizontal axis of 1 s/div and (b) reactive power with the vertical axis of 0.5 kvar/div and the horizontal axis of 1 s/div.

damping ratio expressed in (44), thus conforming to the optimal damping ratio of the second-order system (see [44]).

$$\xi = \frac{k_2}{2\sqrt{ak_1}} = \frac{\sqrt{2}}{2}.\tag{44}$$

Based on the parameters of the test rig elaborated in Subsection V-A in the following section, power response curves under different control parameters are captured and displayed in Fig. 3—which reveals that the larger the $\frac{q}{r}$, the faster the response time. In addition, different control parameters will not affect the damping ratio of the system. Figure 3 reveals that in the method proposed in this paper, modifying different weights will improve the response speed and configure any reasonable dynamics of interest accordingly. Therefore, any reasonably appropriate time constant and interested time response required for controlling active and reactive power in power systems will be achieved.

V. EXPERIMENTS AND SIMULATIONS

Subsection V-A in this section presents the results of the experiments conducted on a VSG connected to a grid made by voltage sources shown in Fig 1. Also, Subsection V-B depicts the simulation results of a VSG connected to power systems based on synchronous generators (SGs). In both subsections, Method 1, Method 2, Method 3, and Method 4 represent the conventional VSG methodology, the virtual impedance increase approach (see [40], [45] for details), the method proposed in [40] (under the virtual impedance increase condition), and the method introduced in this paper, respectively.

A. Experimental Results of A VSG Connected to A Grid Based on Voltage Sources

The test rig depicted in Fig. 4 has been utilized to conduct experimental examinations related to the VSC simulated in this



Fig. 4. Test rig employed in the experiments conducted in the Laboratory for Advanced Power and Energy Systems (LAPES) at Georgia Southern University—where the test rig has been housed.

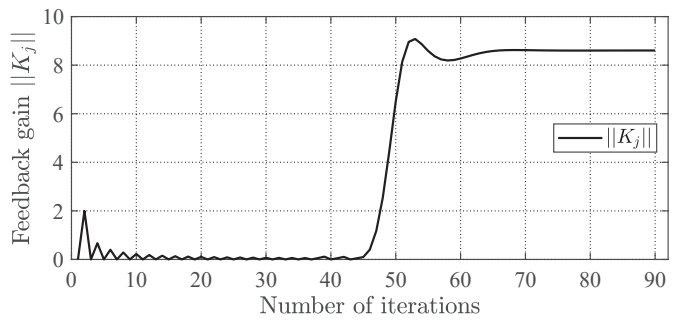


Fig. 5. Convergence of optimal feedback gain K_j during the learning process.

section. It is based on the "SKM 50 GB 123 D" intelligent insulated gate bipolar transistor (also known as IGBT) power modules manufactured by the SEMIKRON company. Besides, SEMIKRON "SKHI 21A (R)" gate drives and protection circuitry are employed to make the converter functional. The Verivolt "IsoBlock I-ST-1c"/"IsoBlock V-1c" current/voltage sensors have been hooked to digital inputs to measure the currents and the voltages, respectively. dSPACE "MicroLabBox (MLBX)" using a real-time processor, field-programmable gate arrays, and different inputs/outputs channels connects the VSC under test to the measurement and drive circuitry. The VSG mentioned above has the parameters of $V_{\rm DC} = 500$ V, $L_f = 4$ mH, $R_f = 0.056$ Ω , C = 50 μF , and $\omega = 314.159$ rad/s and is connected to the Spitzenberger & Spies power amplifiers (APS types) emulating the grid shown in the upper part of Fig. 1

Fig. 5 illustrates the convergence of the optimal feedback gain K_j via Algorithm 2. The results show that the feedback gain obtained in Algorithm 2 can be equivalent to the optimal feedback gain after 90 iterations. Now that the proposed method has been entirely synthesized, the experiments are conducted on different test cases elaborated below. The experimental results show the outcome of Methods 1–4.

$$K_{90} = \begin{bmatrix} 0.0032 & 8.5451 \end{bmatrix}.$$
 (45)

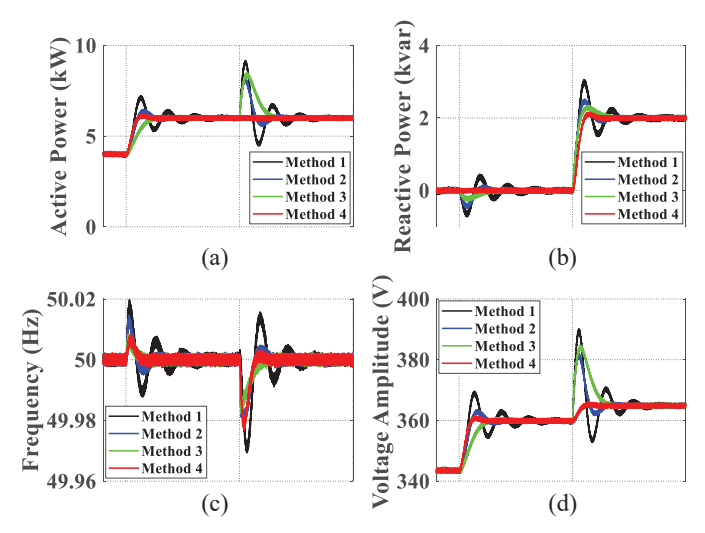


Fig. 6. Comparative experimental results associated with Test Case I for different control methods: (a) active power, (b) reactive power, (c) frequency, and (d) voltage amplitude—vertical axes of Figs. 6(a)–(d) display the unit per division of each with the horizontal axis of 5 s/div for all.

1) Test Case I (Changes in Power Command): The initial power set points are $P_{\text{ref}} = 4 \text{ kW}$ and $Q_{\text{ref}} = 0 \text{ kVar}$. After 5 s, the active power changes to $P_{\text{ref}} = 6 \text{ kW}$, and after another 5 s, the reactive power changes to $Q_{\text{ref}} = 2 \text{ kVar}$. Figure 6 depicts the relevant experimental results, as discussed in Test Case I.

When the active power changes, the following results are captured. Method 1 shows a noticeable overshoot and oscillations. Method 2 effectively reduces the fluctuations in the form of undershoots and overshoots. Method 3 eliminates the system's oscillation but results in a slow response time. Method 4 eliminates the oscillation and has a fast response time. When the reactive power abruptly changes, because the reactive power directly controls the voltage, the voltage abruptly changes, so the active power also changes. Thus, Figs. 6 (a) and (d) display that the output active power and voltage of Methods 1, 2, and 3 have large overshoots after a sudden change in the reactive power. The output active power of Method 4 remains unchanged, and the output voltage steadily increases.

2) Test Case II (Changes in Grid Frequency): The initial power points are $P_{\rm ref}=4$ kW and $Q_{\rm ref}=0$ kVar. After 5 s, the grid frequency is reduced by 0.05 Hz for 5 s. The relevant experimental results are shown in Fig. 7. When the grid frequency changes, the outputs of Methods 1 and 2 make certain oscillations. Method 3 has no oscillation but has a large steady-state deviation. The output active power and voltage of Method 4 increase steadily with satisfactory performance.

The effectiveness of the method proposed herein is also verified and simulated under different frequency changes. Therefore, this paper provides the experimental results under various frequency deviations ($\Delta f = \pm 0.05$ Hz, ± 0.1 Hz, ± 0.15 Hz, and ± 0.2 Hz), and Fig. 8 shows the relevant experiment outcomes. Considering the experimental results, the greater the frequency deviation, the greater the overshoot of the output active and reactive power. Still, the maximum reactive power does not exceed ± 1 kvar, and the active power

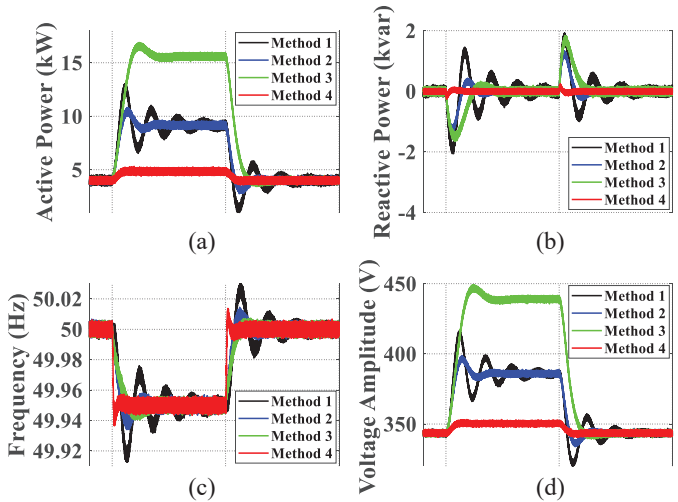


Fig. 7. Comparative experimental results associated with Test Case II for different control methods: (a) Active power, (b) reactive power, (c) frequency, and (d) voltage amplitude—vertical axes of Figs. 7(a)—(d) display the unit per division of each with the horizontal axis of 5 s/div for all.

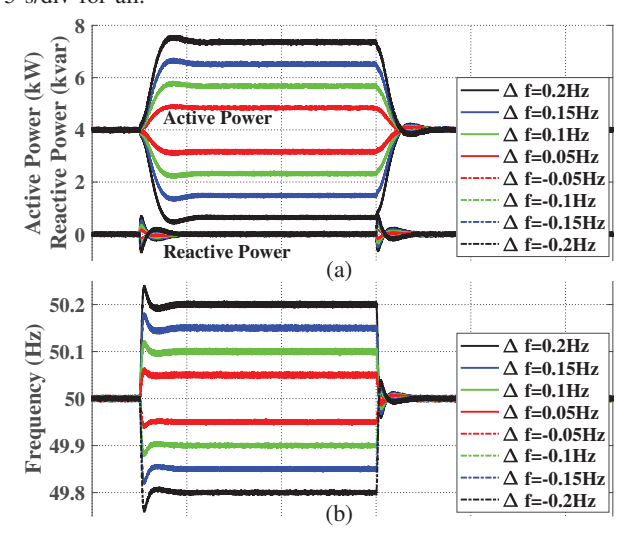


Fig. 8. Comparative experimental results associated with Test Case II for Method 4 under various frequency deviations: (a) Active and reactive power and (b) frequency—vertical axes of Figs. 8(a) and (b) display the unit per division of each with the horizontal axis of 2 s/div for both.

deviation remains stable.

3) Test Case III (Changes in Resistance-to-Inductance Ratio and Weight Matrix): In order to verify the ADP algorithm's effectiveness, experiments are conducted under different resistance-to-inductance ratio ($m \triangleq R_g/\omega_g L_g = 1, 2, 3$, and 4); Fig. 9 shows the results. As the resistance-to-inductance ratios increases, the correlation between the active power and the frequency decreases; nevertheless, the correlation between the reactive power and the frequency increases. When the active power changes, the greater the resistance-to-inductance ratio of the line, the slower the response and the smaller the frequency change. When the reactive power changes, the greater the resistance-to-inductance ratio of the line, the slower the response and the greater the frequency change.

For different weight matrices, i.e., $Q = 10^{-6} \times I_2$, $5 \times 10^{-6} \times I_2$, $10^{-5} \times I_2$, and $5 \times 10^{-5} \times I_2$, the relevant experimental

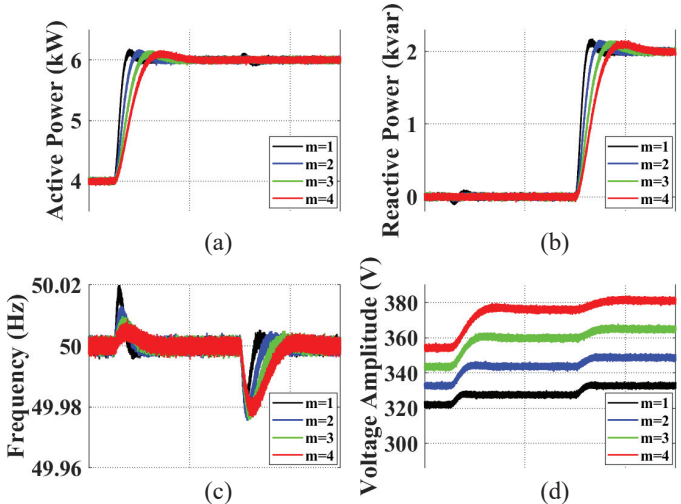


Fig. 9. Comparative experimental results associated with Test Case III for Method 4 under different m values ($m \triangleq R_g/\omega_g L_g$): (a) Active power, (b) reactive power, (c) frequency, and (d) voltage amplitude—vertical axes of Figs. 9(a)–(d) display the unit per division of each with the horizontal axis of 1 s/div for all.

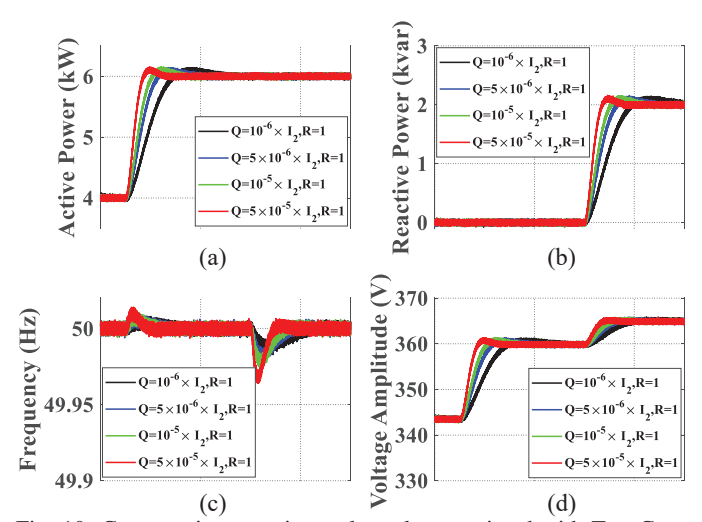


Fig. 10. Comparative experimental results associated with Test Case III for Method 4 under different "Q"s: (a) Active power, (b) reactive power, (c) frequency, and (d) voltage amplitude—vertical axes of Figs. 10(a)–(d) display the unit per division of each with the horizontal axis of 1 s/div for all.

results are shown in Fig. 10. As the weight matrix Q increases, the real part of the eigenvalue decreases [see (43)], thus speeding up the response time. Additionally, because the power angle remains the same, the faster the response, the larger the frequency overshoot. Finally, Fig. 11 displays Phase A of the voltage and current waveforms associated with one of the Test Case III scenarios, i.e., for m=1, just as an example.

B. Simulation Results of A VSG Connected to A Grid Based on Synchronous Generators

In order to verify whether the algorithm proposed in this article is able to typically work in power systems with synchronous generators (SGs), this subsection simulates the voltages of a grid made by an actual SG, thus effectively emulating SG-enabled power systems. Two cases of large

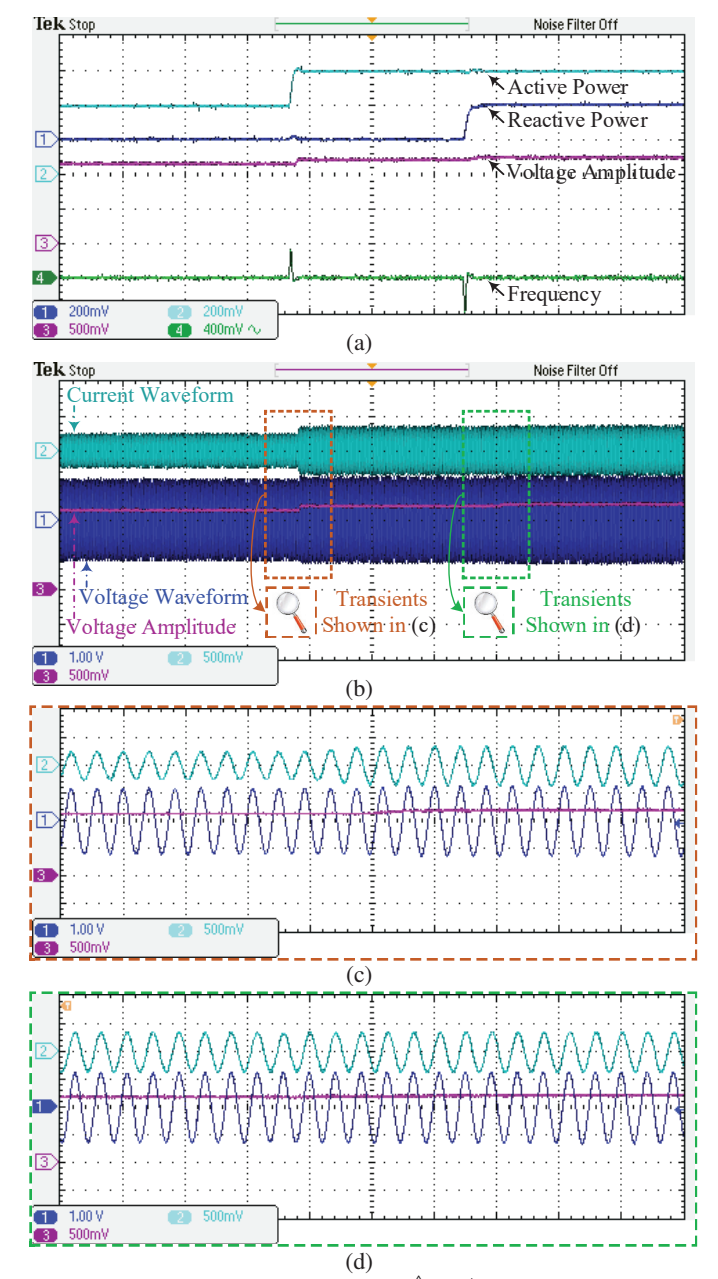


Fig. 11. Experimental results for $m \triangleq R_g/\omega_g L_g$ =1: (a) Reactive power (Ch #1: 2 kvar/div), active power (Ch #2: 2 kW/div), voltage amplitude (Ch #3: 136 V/div), and frequency signal's ac component, i.e., deviation from 50 Hz (Ch #4: 0.02 Hz/div) all with horizontal axis of 1 s/div; (b) voltage waveform (Ch #1: 68 V/div), current waveform (Ch #2: 18 A/div), voltage amplitude (Ch #3: 136 V/div) all with horizontal axis of 1 s/div; (c) information of vertical axes are similar to those in Fig 11(b) but all with horizontal axis of 40 ms/div; and (d) information of vertical and horizontal axes are similar to those in Fig 11(c).

and small power systems are simulated; they include two SGs with two various nominal power/nominal voltage of 200 and 0.5 MVA/400 and 13500 V (with relevant connecting transformers), and those SGs have the inertia coefficient of H=0.6 s and the internal impedances of R=0.0036 per unit (pu) and X=0.16 pu. Figures 12 and 13 present simulation results associated with different control methods for SGs with two nominal power values to be able to emulate practical SG-enabled power systems effectively.

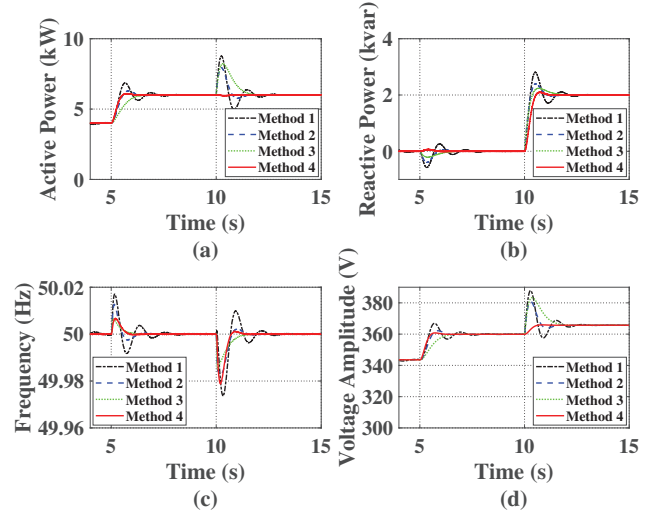


Fig. 12. Comparative simulation results associated with different control methods for a 200-MVA, 13800-V SG: (a) active power, (b) reactive power, (c) frequency, and (d) voltage amplitude.

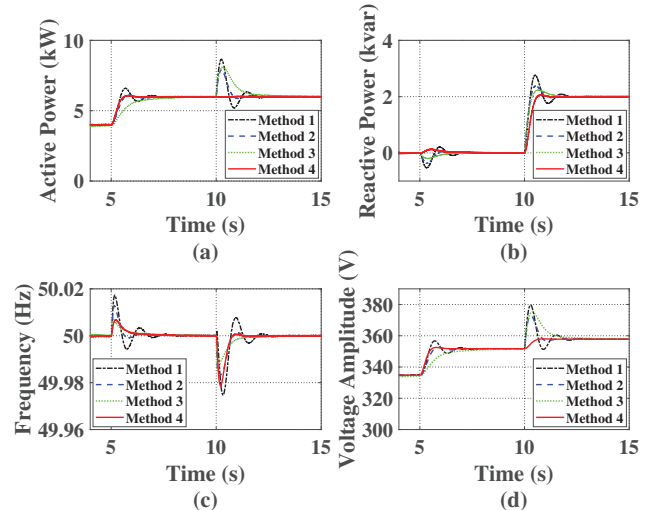


Fig. 13. Comparative simulation results associated with different control methods under a 0.5-MVA, 400-V SG: (a) active power, (b) reactive power, (c) frequency, and (d) voltage amplitude.

VI. CONCLUSION

This study has proposed an improved VSG control based on ADP. Also, it has relaxed the conditions where the line impedance is inductive and the power angle is approximately zero. Furthermore, this study has addressed the coupling between the active and reactive power by regarding the model's nonlinear dynamics as disturbances and synthesizing the optimal feedback control and compensation controller via the linear ADP method. It has also eliminated the influence of frequency fluctuation. The proposed model-free method has been compared to the conventional VSG control method. The comparative experimental results herein have shown that the designed control has reduced the system's oscillation, decreased the coupling between the active and reactive power, and improved the overall control performance when the impedance of the connecting line is not purely inductive and when the system parameters are unknown. Furthermore, according to the experiments conducted, the proposed ADP control has displayed improvements in performance and effects in case of power grid frequency fluctuation in power grid voltage.

REFERENCES

- [1] S. Yazdani, M. Davari, M. Ferdowsi, and P. Shamsi, "Internal model power synchronization control of a PV-based voltage-source converter in weak-grid and islanded conditions," *IEEE Trans. Sustain. Energy*, vol. 12, no. 2, pp. 1360–1371, Apr. 2021.
- [2] M. Davari and Y. A.-R. I. Mohamed, "Robust DC-link voltage control of a full-scale PMSG wind turbine for effective integration in DC grids," *IEEE Trans. Power Electron.*, vol. 32, no.5, pp.4021–4035, May 2017.
- [3] M. Davari and Y. A.-R. I. Mohamed, "Robust droop and DC-bus voltage control for effective stabilization and power sharing in VSC multiterminal DC grids," *IEEE Trans. Power Electron.*, vol. 33, no.5, pp. 4373–4395, May 2018.
- [4] X. Wang, Z. Lv, R. Wang, and X. Hui, "Optimization method and stability analysis of MMC grid-connect control system based on virtual synchronous generator technology," *Electr. Power Syst. Res.*, vol. 182, pp. 106209, May 2020.
- [5] J. Liu, Y. Miura, and T. Ise, "Comparison of dynamic characteristics between virtual synchronous generator and droop control in inverterbased distributed generators," *IEEE Trans. Power Electron.*, vol. 31, no. 5, pp. 3600–3611, May 2015.
- [6] R. V. Ferreira, S. M. Silva, H. Antunes, and G. Venkataramanan, "Dynamic analysis of grid-connected droop-controlled converters and synchronverters," *J. Control Autom. Electr. Syst.*, vol. 30, no. 5, pp. 741–753, Oct. 2019.
- [7] N. D. Tuyen, G. Fujita, T. Funabashi, and M. Nomura, "Analysis of transient-to-island mode of power electronic interface with conventional dq-current controller and proposed droop-based controller," *Electr. Eng.*, vol. 99, no. 1, pp. 47–57, Mar. 2017.
- [8] J. Chen, M. A. Liu, X. Chen, B. W. Niu, and C. Y. Gong, "Wireless parallel and circulation current reduction of droop-controlled inverters," *Trans. Chin. Electrotech. Soc.*, vol. 33, pp. 1450–1460, 2018.
- [9] J. Alipoor, Y. Miura, and T. Ise, "Power system stabilization using virtual synchronous generator with alternating moment of inertia," *IEEE J. Emerg. Sel. Topics Power Electron.*, vol. 3, no. 2, pp. 451–458, Jun. 2015.
- [10] M. Li, W. Huang, N. Tai, and D. Duan, "Virtual inertia control of the virtual synchronous generator: A review," arXiv:2109.07590v1, submitted on 15 Sep. 2021, doi: 10.48550/arXiv.2109.07590.
- [11] D. Li, Q. Zhu, S. Lin, and X. Y. Bian, "A self-adaptive inertia and damping combination control of VSG to support frequency stability," *IEEE Trans. Energy Convers.*, vol. 32, no. 1, pp. 397–398, Mar. 2017.
- [12] F. Wang, L. Zhang, X. Feng, and H. Guo, "An adaptive control strategy for virtual synchronous generator," *IEEE Trans. Ind. Appl.*, vol. 54, no. 5, pp. 5124–5133, Sep./Oct. 2018.
- [13] F. H. Xu, C. Yu, C. Liu, and Q. Wang, "An improved virtual inertia algorithm of virtual synchronous generator," J. Mod. Power Syst. Clean Energy, vol. 8, no. 2, pp. 377–386, Mar. 2020.
- [14] S. Barcellona, Y. Huo, R. Niu, L. Piegari, and E. Ragaini, "Control strategy of virtual synchronous generator based on virtual impedance and band-pass damping," 2016 International Symposium on Power Electronics, Electrical Drives, Automation and Motion (SPEEDAM). IEEE, pp. 1354–1362, 2016.
- [15] W. Ma, Y. Guan, and B. Zhang, "Active disturbance rejection control based control strategy for virtual synchronous generators," *IEEE Trans. Energy Convers.*, vol. 35, no. 4, pp. 1747–1761, Dec. 2020.
- [16] B. Long, Y. Liao, K. T. Chong, J. Rodríguez, and J. M. Guerrero, "MPC-controlled virtual synchronous generator to enhance frequency and voltage dynamic performance in islanded microgrids," *IEEE Trans. Smart Grid*, vol. 12, no. 2, pp. 953–964, Mar. 2021.
- [17] J. W. Simpson-Porco, Q. Shafiee, F. Dörfler, J. C. Vasquez, J. M. Guerrero, and F. Bullo, "Secondary frequency and voltage control of islanded microgrids via distributed averaging," *IEEE Trans. Ind. Electron.*, vol. 62, no. 11, pp. 7025–7038, Nov. 2015.
- [18] Y. Xu, H. Sun, W. Gu, Y. Xu, and Z. Li, "Optimal distributed control for secondary frequency and voltage regulation in an islanded microgrid," *IEEE Trans. Ind. Inform.*, vol. 15, no. 1, pp. 225–235, Jan. 2019.
- [19] C. Peng, J. Zhang, and H. Yan, "Adaptive event-triggering H_∞ load frequency control for network-based power systems," *IEEE Trans. Ind. Electron.*, vol. 65, no. 2, pp. 1685–1694, Feb. 2018.
- [20] M. Davari, M. P. Aghababa, F. Blaabjerg, and M. Saif, "A modular adaptive robust nonlinear control for resilient integration of VSIs into emerging modernized microgrids," *IEEE J. Emerg. Sel. Topics Power Electron.*, vol. 9, no. 3, pp. 2907–2925, Jun. 2021.

- [21] M. Davari and Y. A.R.-I Mohamed, "Robust vector control of a very weak-grid-connected voltage-source converter considering the phaselocked loop dynamics," *IEEE Trans. Power Electron.*, vol. 32, no. 1, pp. 977–994, Feb. 2017.
- [22] T. Wen, X. Zou, D. Zhu, X. Guo, L. Peng, and Y. Kang, "Comprehensive perspective on virtual inductor for improved power decoupling of virtual synchronous generator control," *IET Renew. Power Gener.*, vol. 14, no. 4, pp. 485–494, Mar. 2020.
- [23] Y. Yang, J. Xu, C. Li, W. Zhang, Q. Wu, M. Wen, and F. Blaabjerg, "A new virtual inductance control method for frequency stabilization of grid forming virtual synchronous generators," *IEEE Trans. Ind. Electron.*, vol. 70, no. 1, pp. 441–451, Jan. 2023.
- [24] M. Li, Y. Wang, N. Xu, W. Wang, and Y. Liu, "A power decoupling control strategy for droop controlled inverters and virtual synchronous generators," in *Proc. of the IEEE 8th International Power Electronics* and Motion Control Conference (IPEMC-ECCE Asia), 2016, pp. 1713– 1719
- [25] Y. Li and Y. W. Li, "Power management of inverter interfaced autonomous microgrid based on virtual frequency-voltage frame," *IEEE Trans. Smart Grid*, vol. 2, no. 1, pp. 30–40, Mar. 2011.
- [26] B. Li, L. Zhou, X. Yu, C. Zheng, and J. Liu, "Power decoupling method based on the diagonal compensating matrix for VSG-controlled parallel inverters in the microgrid," *Energies*, vol. 10, no. 12, pp. 2159–2171, 2017
- [27] Y. Li and Y. W. Li, "Improved power decoupling control strategy based on virtual synchronous generator," *IET Power Electron.*, vol. 10, no. 4, pp. 462–470, Jan. 2017.
- [28] M. Li, Y. Wang, N. Xu, Y. Liu, W. Wang, H, Wang, and W. Lei, "A novel virtual synchronous generator control strategy based on improved swing equation emulating and power decoupling method," in *Proc. of* the IEEE Energy Conversion Congress and Exposition (ECCE), 2016, pp. 1–7.
- [29] A. B. Ataji, Y. Miura, T. Ise, and H. Tanaka, "A new robust decoupled control of the stator active and reactive currents for grid-connected doubly-fed induction generators," *Energies*, vol. 9, no. 3, p. 179, pp. 1–18, Mar. 2016, doi: 10.3390/en9030179.
- [30] R. S. Sutton and A. G. Barto, "Reinforcement learning: An introduction," Cambridge, MA, USA: MIT Press, 2018.
- [31] S. Wu, W. Hu, Z. Lu, Y. Gu, and B. Tian, "Power system flow adjustment and sample generation based on deep reinforcement learning," *J. Mod. Power Syst. Clean Energy*, vol. 8, no. 6, pp. 1115–1127, Nov. 2020.
- [32] O. Nassef, L. Sequeira, E. Salam, and T. Mahmoodi, "Building a lane merge coordination for connected vehicles using deep reinforcement learning," *IEEE Internet Things J.*, vol. 8, no. 4, pp. 2540–2557, Feb. 15, 2020.
- [33] Z. Bing, H. Zhou, R. Li, X. Su, F. O. Morin, K. Huang, and A. Knoll, "Solving robotic manipulation with sparse reward reinforcement learning via graph-based diversity and proximity," *IEEE Trans. Ind. Electron.*, vol. 70, no. 3, pp. 2759–2769, Mar. 2023.
- [34] Y. Jiang and Z. -P. Jiang, "Global adaptive dynamic programming for continuous-time nonlinear systems," *IEEE Trans. Autom. Control*, vol. 60, no. 11, pp. 2917–2929, Nov. 2015.
- [35] Q. Wei, Z. Liao, R. Song, P. Zhang, Z. Wang, and J. Xiao, 'Self-learning optimal control for ice-storage air conditioning systems via data-based adaptive dynamic programming," *IEEE Trans. Ind. Electron*, vol. 68, no. 4, pp. 3599–3608, Apr. 2021.
- [36] W. Gao and Z.-P. Jiang, "Adaptive dynamic programming and adaptive optimal output regulation of linear systems," *IEEE Trans. Autom. Control*, vol. 61, no. 12, pp. 4164–4169, Dec. 2016.
- [37] W. Gao, Y. Jiang, Z.-P. Jiang, and T. Chai, "Output-feedback adaptive optimal control of interconnected systems based on robust adaptive dynamic programming," *Automatica*, vol. 72, pp. 37–45, Dec. 2016.
- [38] B. Luo, Y. Yang, and D. Liu, "Policy iteration Q-Learning for data-based two-player zero-sum game of linear discrete-time systems," *IEEE Trans. Cybern.*, vol. 51, no. 7, pp. 3630–3640, Jul. 2021.
- [39] T. Bian and Z.-P. Jiang, "Value iteration and adaptive dynamic programming for data-driven adaptive optimal control design," *Automatica*, vol. 71, pp. 348–360, Sep. 2016.
- [40] Z. Wang, Y. Yu, W. Gao, M. Davari, and C. Deng, "Adaptive, optimal, virtual synchronous generator control of three-phase grid-connected inverters under different grid conditions—An adaptive dynamic programming approach," *IEEE Trans. Ind. Inform.*, vol. 18, no. 11, pp. 7388–7399, Nov. 2022.
- [41] Y. Zhang, Q. Sun, J. Zhou, J. M. Guerrero, R. Wang, and A. Lashab, "Optimal frequency control for virtual synchronous generator based AC microgrids via adaptive dynamic programming," *IEEE Trans. Smart Grid*, vol. 14, no. 1, pp. 4–16, Jan. 2023.

- [42] T. Wen, D. Zhu, X. Zou, B. Jiang, L. Peng, and Y. Kang, "Power coupling mechanism analysis and improved decoupling control for virtual synchronous generator," *IEEE Trans. Power Electron.*, vol. 36, no. 3, pp. 3028–3041, Mar. 2021.
- [43] U. Markovic, Z. Chu, P. Aristidou, and G. Hug, "LQR-based adaptive virtual synchronous machine for power systems with high inverter penetration," *IEEE Trans. Sustain. Energy*, vol. 10, no. 3, pp. 1501– 1512, Jul. 2019.
- [44] S. M. Shahruz, G. Langari, and M. Tomizuka, "Optimal damping ratio for linear second-order systems," *Journal of Optimization Theory and Applications*, vol. 73 (1992), pp. 563–576, 1992.
- [45] T. Wen, X. Zou, D. Zhu, X. Guo, L. Peng, and Y. Kang, "Comprehensive perspective on virtual inductor for improved power decoupling of virtual synchronous generator control," *IET Renew. Power Gener.*, vol. 14, no.4, pp. 485–494, Mar. 2020.



Zhongyang Wang was born in Chuzhou, China. He received the B.Sc. degree in Automation from the East China University of Technology in 2017 and the M.Sc. degree in Control Science and Engineering from the Nanchang University in 2020. He is currently pursuing the Ph.D degree at Beijing University of Chemical Technology, Beijing. His research interests include adaptive dynamic programming, optimal control of linear systems, and control of power systems.



Youqing Wang (Senior Member, IEEE) received the B.S. degree in mathematics from Shandong University, Jinan, Shandong, China, in 2003, and the Ph.D. degree in control science and engineering from Tsinghua University, Beijing, China, in 2008.

He worked chronologically at The Hong Kong University of Science and Technology, Hong Kong, China; the University of California at Santa Barbara, Santa Barbara, CA, USA; the University of Alberta, Edmonton, AB, Canada; the Shandong University of Science and Technology, Qingdao, Shandong; and

the City University of Hong Kong, Hong Kong. He is currently a Professor with the Beijing University of Chemical Technology, Beijing. His research interests include fault diagnosis, fault-tolerant control, state monitoring, and iterative learning control for chemical and biomedical processes.

Dr. Wang was a recipient of several honors and awards, including the IET Fellow, the NSFC Distinguished Young Scientists Fund, the *Journal of Process Control* Survey Paper Prize, and the ADCHEM2015 Young Author Prize.



Masoud Davari (Senior Member, IEEE) was born in Isfahan, Iran, on September 14, 1985. He received the B.Sc. degree (summa cum laude) in electrical engineering (power) from the Isfahan University of Technology, Isfahan, in 2007, the M.Sc. degree (summa cum laude) in electrical engineering (power) from the Amirkabir University of Technology (Tehran Polytechnic), Tehran, Iran, in 2010, and the Ph.D. degree in electrical engineering (power electronics in energy systems with distinction/honors) from the University of Alberta,

Edmonton, AB, Canada, in 2016.

He was with Iran's Grid Secure Operation Research Center and Iran's Electric Power Research Institute (EPRI), Tehran, Iran, from January 2010 to December 2011. From April 2015 to June 2017, he was a Senior R & D Specialist and Senior Consultant with Quanta-Technology Company, Markham, ON, Canada, in the field of the dynamic interaction of renewables with smart ac/dc grids and control, protection, and automation of microgrids. In July 2017, he joined as a tenure-track Assistant Professor with the Allen E. Paulson College of Engineering and Computing, Department of Electrical and Computer Engineering, Georgia Southern University (GSU), Statesboro, GA, USA—where he was recommended for being granted "early" promotion to Associate Professor and award of "early" tenure on December 3, 2021, and officially approved for both on February 16, 2022. He is the founder

and the director of the Laboratory for Advanced Power and Energy Systems [LAPES (watch it on https://www.youtube.com/watch?v=mhVHp7uMNKo)] in the state-of-the-art Center for Engineering and Research (CEaR) established in 2021 with GSU. He has developed and implemented several experimental test rigs for research universities and the power and energy industry. He has also authored several papers published in IEEE Transactions and journals. His research interests include the dynamics, controls, and protections of different power electronic converters utilized in the hybrid ac/dc smart grids, and hardware-in-the-loop (HIL) simulation-based testing of modernized power systems.

Dr. Davari has been an active member and a chapter lead in the IEEE Power & Energy Society Task Force on "Innovative Teaching Methods for Modern Power and Energy Systems" since July 2020. He has been an active member and a chapter lead (for Chapter 3) in the IEEE Working Group P2004-a newly established IEEE working group entitled "Hardware-in-the-Loop (HIL) Simulation Based Testing of Electric Power Apparatus and Controls" for IEEE Standards Association since June 2017. He is an invited member of the Golden Key International Honour Society. He was the Chair of the Literature Review Subgroup of DC@Home Standards for the IEEE Standards Association from April 2014 to October 2015. He is an invited reviewer of several of the IEEE TRANSACTIONS/JOURNALS, IET journals, Energies journal, and various IEEE conferences, the invited speaker at different universities and in diverse societies, and the Best Reviewer of the IEEE TRANSACTIONS ON POWER SYSTEMS in 2018 and 2020. He is the recipient of the 2019-2020 Allen E. Paulson College of Engineering and Computing (CEC) Faculty Award for Outstanding Scholarly Activity in the Allen E. Paulson CEC at GSU, the Discovery & Innovation Award from the 2020-2021 University Awards of Excellence at GSU, and one of the awardees of the 2021-2022 Impact Area Accelerator Grants (partially funded) at GSU.



Frede Blaabjerg (Fellow, IEEE) received the Ph.D. degree in electrical engineering from Aalborg University, Aalborg, Denmark, in 1995. From 1987 to 1988, he was with ABBScandia, Randers, Denmark. He became an Assistant Professor, an Associate Professor, and a Full Professor of power electronics and drives with Aalborg University, in 1992, 1996, and 1998, respectively. In 2017, he became a Villum Investigator. Additionally, he is Honoris Causa with University Politehnica Timisoara (UPT), Timisoara, Romania, and Tallinn Technical University, Tallin,

Estonia. He has authored or coauthored four monographs, published more than 600 journal articles in the fields of power electronics and its applications and was an editor of ten books in power electronics and its applications. His current research interests include power electronics and its applications, such as in wind turbines, PV systems, reliability, harmonics, and adjustable speed drives. He was a recipient of the 33 IEEE Prize Paper Awards, the IEEE PELS Distinguished Service Award in 2009, the EPE-PEMC Council Award in 2010, the IEEE William E. Newell Power Electronics Award 2014, the Villum Kann Rasmussen Research Award 2014, the Global Energy Prize in 2019, and the 2020 IEEE Edison Medal. From 2006 to 2012, he was the Editor-in-Chief for the IEEE TRANSACTIONS ON POWER ELECTRONICS. From 2005 to 2007, he was a Distinguished Lecturer of the IEEE Power Electronics Society and the IEEE Industry Applications Society from 2010 to 2011 and from 2017 to 2018. From 2019 to 2020, he was the President of IEEE Power Electronics Society. He was the Vice President of the Danish Academy of Technical Sciences, Lyngby, Denmark. From 2014 to 2020, he was nominated by Thomson Reuters, Toronto, Canada, to be between the most 250 cited researchers in engineering in the world.